

# Gold nanorods as molecular contrast agents in photoacoustic imaging: the promises and the caveats

Srirang Manohar,\* Constantin Ungureanu, and Ton G. Van Leeuwen†

*Biomedical Photonic Imaging Group,  
MIRA Institute for Biomedical Technology and Technical Medicine,  
Faculty of Science and Technology,  
University of Twente, P.O. Box 217,  
7500 AE Enschede, The Netherlands*

(Dated: February 13, 2011)

## Abstract

Rod-shaped gold nanoparticles exhibit intense and narrow absorption peaks for light in the far-red and near-infrared wavelength regions, due to the excitation of longitudinal plasmons. Light absorption is followed predominantly by non-radiative de-excitation, and the released heat and subsequent temperature rise cause strong photoacoustic (optoacoustic) signals to be produced. This feature combined with the relative inertness of gold, and its favorable surface chemistry which permits affinity biomolecule coupling, has seen gold nanorods (AuNR) attracting much attention as contrast agents and molecular probes for photoacoustic imaging. In this article we provide an short overview of the current status of the use of AuNR in molecular imaging using photoacoustics. We further examine the state-of-the-art in various chemical, physical and biochemical phenomena that have implications for the future photoacoustic applications of these particles. We cover the route from fine-tuning of AuNR synthetic procedures, toxicity reduction by appropriate coatings, *in vitro* cellular interactions of AuNRs, attachment of targeting antibodies, *in vivo* fate of the particles and the effects of certain light interactions with the AuNR.

---

\* S.Manohar@utwente.nl

† Also at Biomedical Engineering and Physics, Academic Medical Center, University of Amsterdam, P.O. Box 2270, 1100 DE Amsterdam, The Netherlands

## I. BACKGROUND

Fine particles of noble metals in the nanometric size range possess intense and spectrally narrow absorption and scattering peaks in their interactions with light [1]. This feature endows dispersions of these nanoparticles with vivid colors, a property that was recognized early on by craftsmen in the Middle Ages (and perhaps earlier - see Ref. [2]), who used gold, silver and alloyed powders in glass to make stained glass window panels with distinctive reds, purples and yellows. In 1857 Michael Faraday developed the first scientific underpinnings to these observations with his experiments on light interactions with metal particles “minute in their dimensions” [3]. He had been especially fascinated by the ruby-red appearance of gold dispersions in water. In 1908, Gustav Mie [4] laid the mathematical foundation which could be used to explain the dependence of the optical properties on the sizes of finely divided gold. Mie solved Maxwell’s equations for light interaction with small spheres [5]. The material of the sphere possesses a complex frequency-dependent dielectric function  $\epsilon(\omega)=\epsilon_1(\omega) + i\epsilon_2(\omega)$ , and the embedding material is water with a frequency-independent dielectric function  $\epsilon_m$ . From Mie’s theory, under the dipole approximation, the extinction cross-section  $\sigma_e(\omega)$  is given by:

$$\sigma_e(\omega) \propto \frac{\omega \epsilon_m^{3/2} \epsilon_2(\omega)}{[\epsilon_1(\omega) + 2\epsilon_m]^2 + \epsilon_2(\omega)^2} \quad (1)$$

For a certain frequency of light,  $\epsilon_1$  achieves a value equal to  $-2\epsilon_m$  which causes  $\sigma_e$  to ‘blow up’ [5]. Gold spheres smaller than 20 nm achieve this resonance condition at 516 nm in the green region of the spectrum, which explains the ruby-red color of gold nanospheres [6].

A physical meaning can be obtained by considering that the free electrons of the noble metal interact electrostatically forming an electron plasma which can be excited by light of the appropriate energy to perform fluid-like oscillations [7]. This plasma possesses, just like an oscillator, a resonance frequency. In quantum mechanical parlance one says that a localized surface plasmon (LSPR) is excited at resonance. In the case of gold at the nanoscale, the boundaries confine the oscillation and resonance occurs at the visible frequencies. At this wavelength, light is most effectively coupled to the metal particle and the interaction (absorption and/or scattering) will peak.

If the geometrical symmetry of the gold particle is disturbed from the spherical, with elongation of the particle in one direction, plasmons can be excited along the two available axes for a scrambled polarization of light. Oscillations directed along the short axis give rise

to an interaction peak called the transverse plasmon (TP) peak, oscillations along the major axis give rise to a lower energy longitudinal plasmon (LP) peak. The spectral location of the TP peak remains relatively fixed around 516 nm, while the LP peak position is sensitive to the aspect ratio (AR) of the particle; the higher the AR the higher is the red-shift [5]. Such nanoparticles in the form of hemispherically-capped cylinders called nanorods (NRs) can be synthesized with an excellent control of aspect ratios providing LP peaks in the red and near-infrared (NIR) wavelengths [8, 9].

The ability to tune the nanorods' strong and narrow LP absorption peak in the range of 650-1100 nm makes the particles attractive for optical imaging in tissue [10]. In this wavelength regime, tissue exhibits as it were, a spectral 'window', where light is able to penetrate fairly deep due to low absorption and low scattering by tissue [11, 12]. Further, the particles' absorbed photon energy is rapidly thermalized by electron-electron collisions and transferred to the lattice by electron-phonon collisions to achieve efficient photothermal conversion [5]. These characteristics make gold nanorods (AuNR) a boon for photoacoustic (also called optoacoustic) imaging, which relies on absorption of pulsed light to generate ultrasound due to rapid heating and thermoelastic expansion. If these AuNRs could be made to accumulate at the disease site of interest, then a sensitive and specific detection/diagnosis of the pathology could be achieved using photoacoustic imaging.

Oraevsky was the first to recognize this potential synergy between AuNRs and photoacoustic imaging, and he advocated as far back as 2001 [13] the use of these particles, among others, as contrast agents in the spirit of molecular imaging. Since then much knowledge has been gained in the photoacoustic imaging community in the use of these [14–26] and other plasmonic nanoparticles such as gold nanoshells [27], nanocages [28, 29] and gold nanobeacons [30]. Photoacoustic (PA) imaging experiments have been conducted using AuNR in phantoms, in cells *in vitro* and in murine/rodent models of disease. Highlights of the small animal *in vivo* work are summarized in the next paragraphs

In 2007, Eghtedari *et al*[19] demonstrated that AuNR could be detected *in vivo* in a mouse using the laser optoacoustic imaging system (LOIS) which employed a 32-element ultrasound detector and pulsed light at 757 nm from an Alexandrite laser. The authors visualized higher signals arising from the presence of PEGylated AuNRs injected subcutaneously into the abdominal region of a nude mouse at the LP peak of the particles. Agarwal *et al*[21] imaged gel beads dispersed with AuNR implanted in the hind leg of a mouse using a hybrid

ultrasound (US)-photoacoustic (PA) system where a clinical ultrasonography system was synchronized to a laser. They obtained co-registered US and PA images, the latter showing the presence of AuNR with anatomical contexts obtained from US. In 2008, the groups of P.-C. Li and C.-R. C. Wang who were active in many aspects of synthesis and applications of AuNR, published the first clear demonstration of molecular imaging using antibody coupled AuNR[23]. They conjugated two samples of AuNRs to anti-EGFR and anti-HER2 antibodies respectively. Two types of tumors were induced in the backs of mice by implantation of oral cancer (OECM1) cells which overexpress HER2 receptors, and squamous cell carcinoma (Cal27) cells which overexpress EGFR receptors. A home-made PA imager using a LiNbO<sub>3</sub> transducer coupled to appropriate lasers was used to show the selectivity that could be obtained using the appropriate targeted AuNR. Figure 1 panel (a) shows an example of an overlay of the pseudocolor PA image on the gray scale US image in the left column, and the PA image in gray scale in the right column of a Cal27 tumor when AuNR<sub>1064</sub>-EGFR are injected into a mouse[23].

In 2009, the group of L.-H. Wang[24] used AuNR as a tracer in PA mapping of lymph drainage to identify sentinel lymph nodes in rat models. The system used was a deeply penetrating PA microscopy system. Cui *et al*[31] also used PA microscopy in 2010 to visualize AuNR accumulated at a tumor site in a mouse model, to guide the application of high-intensity focussed ultrasound (HIFU) for therapy. In the same year, Taruttis *et al*[26] showed real-time imaging of circulating AuNR in blood vessels in the neck region of a mouse injected with the particles. They used a 10 frame per second acquisition system for signals from a 64-element ultrasound detector array with the mouse illuminated from multiple directions to obtain multiple wavelength images using their multispectral technique (MSOT)[32]. Figure 1 panel (b) shows the comparison of the cryosection of the neck region of the mouse with the PA images processed using MSOT of the same region pre- and post-injection of the AuNRs.

Other such feasibility studies have been discussed in a few excellent review articles[33]. In this overview article, we will not tread this path, as this is tantamount to a mere update of the published reviews. Rather we will critically examine the state-of-the-art in various chemical, physical and biochemical phenomena that have crucial implications in the future applications of these particles in PA imaging. The reader will be taken along the trajectory from fine-tuning of AuNR synthetic procedures, toxicity reduction by appropriate NR coatings, *in vitro* cellular interactions of NRs, attachment of targeting antibodies, *in vivo* fate of the

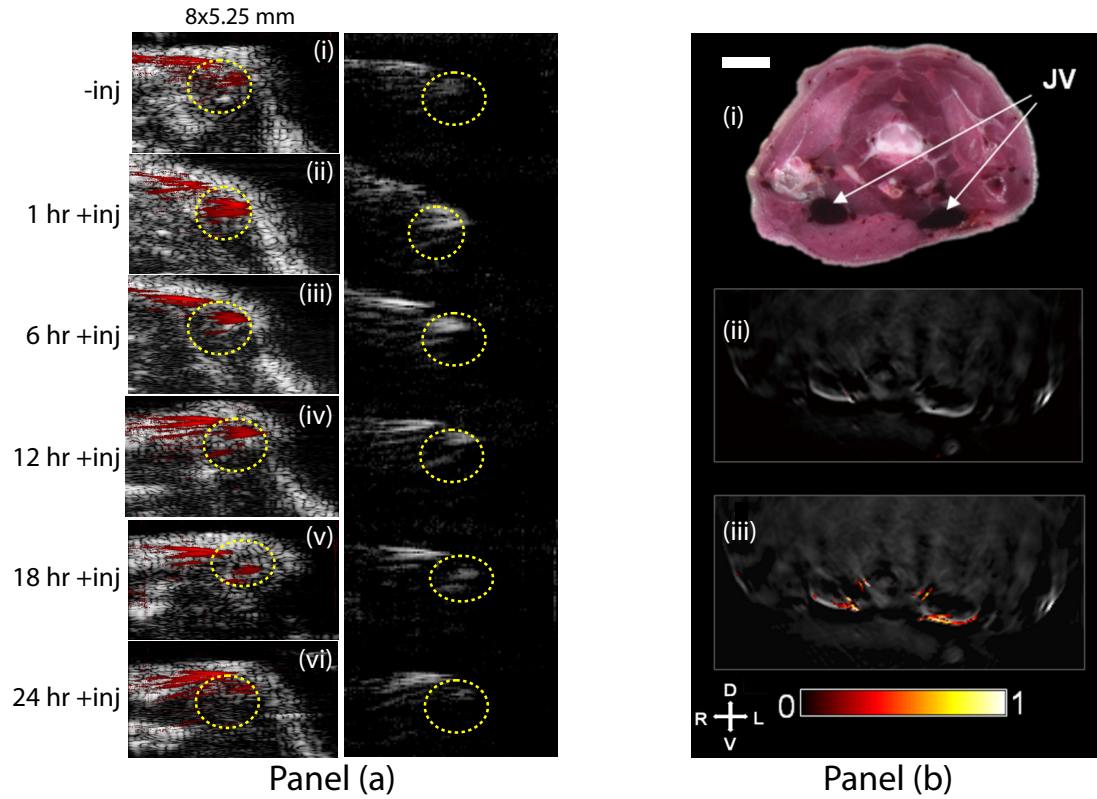


FIG. 1. Panel (a) shows images of Cal27 tumor before and after the injection of AuNR<sub>1064</sub>-EGFR. Ellipses indicate the tumor regions. Left column show fusion images before/after the injection at different time points. The ultrasound images are displayed on a grayscale, and the superimposed PA images obtained at an optical wavelength of 1064 nm are displayed in red pseudocolor. Right column show PA images before/after injection shown in the same scale. (Panel (a) adapted from Ref. [23] with permission from authors and the Optical Society of America (OSA), copyright 2008.) Panel (b): From top to bottom (i) Photograph of cryosection showing anatomical correspondences with jugular veins labeled JV, (ii) Multi Spectral Optoacoustic Tomographic (MSOT) image before injection, (iii) MSOT image post-injection showing multispectrally resolved distribution of AuNR overlaid on a single wavelength image. Scale bar 3 mm. (Panel (b) adapted from Ref. [26] with permission from authors and the Optical Society of America (OSA), copyright 2010.)

particles and the effects of certain light interactions with the AuNR.

## II. SYNTHESIS OF GOLD NANORODS

Rod shaped gold nanoparticles were initially prepared by depositing gold in porous templates using electrochemical and photochemical methods[34]. Attention shifted to wet-chemistry methods with the development of the seeded-growth method by Murphy and co-workers *et al* [35, 36]. Gold spheres were used to seed a growth solution comprising gold salt and ascorbic acid (AA) as a mild reducing agent in the presence of a surfactant cetyltrimethylammonium bromide (CTAB). The latter is thought to form ‘soft’ micellar templates for AuNR formation with medium to high aspect ratios (5-20).

Jana *et al* [37] used silver ions during the seeded-growth procedure, a feature that was further investigated and improved by Nikoobakht and El-Sayed [38] to achieve spectacular yields of AuNR (upto 100% yield up from the 20-40% yield without silver ions) with excellent monodispersity. Importantly, they showed the fine control that was possible in tailoring the aspect ratios (AR) of the AuNR by changing the quantity of  $\text{Ag}^+$  ions in the growth solution. The mechanism at work in this protocol has been debated in the recent past. In solution-phase synthesis the final shape of the nanoparticles is driven by the influence of capping agents [39]. In the case of gold nanorod synthesis, it has been discussed that CTAB (and  $\text{Ag}^+$ ) stabilize the 110 faces to a greater extent than the  $\{100\}$  surfaces of the growing Au seed leading to a faster rate of Au atom growth on the latter, and consequently one-dimensional growth along the  $[100]$  direction [40–42].

### A. The seed-mediated silver assisted protocol

The Nikoobakht and El-Sayed [38] method with small variations [43–46], remains the most popular method for synthesizing AuNRs. We describe briefly our version of the protocol that works well. Figure 1 depicts a schematic of the procedure.

1. Preparation of growth solution: To freshly prepared 0.5 ml of 0.01 M gold salt ( $\text{HAuCl}_4$ ) solution, is added 9.5 ml of 0.1 M CTAB solution with thorough mixing to yield a dark yellow solution. (Flask A in Fig. 1.) Using different  $\text{AgNO}_3$  concentrations in the growth solution allows a tuning of the LP peaks between 650–950 nm. To illustrate the AuNR size and LP wavelength tuning effect of  $\text{AgNO}_3$  we use 8 volumes of 0.01 M of  $\text{AgNO}_3$  (20, 50, 70, 100, 200, 250, 300 and 350  $\mu\text{l}$ ), to provide 8 growth

solutions. To these, 55  $\mu\text{l}$  of 0.1 M ascorbic acid is added with stirring. The resultants turn colorless.

2. Preparation of gold seed: To 0.25 ml of 0.01 M  $\text{HAuCl}_4$  solution, 9.75 ml of 0.1 M CTAB is added with stirring. (Flask B in Fig. 1.) 0.01 M sodium borohydride ( $\text{NaBH}_4$ ) solution in a volume of 0.6 ml is added to the mixture all at once with vigorous stirring for 2 minutes. The resultant is used within about 5 minutes to seed each growth solution.
3. Growth phase: The seed solution is added in a volume of 12  $\mu\text{l}$  to the growth solutions with gentle stirring. The resultants are maintained undisturbed at 25°C for 24 hours. At the bottom of the vessel, a dark-blue suspension is seen with a brownish opalescence. The contents of the vessel are centrifuged and the precipitates re-dispersed in 10 ml of water.

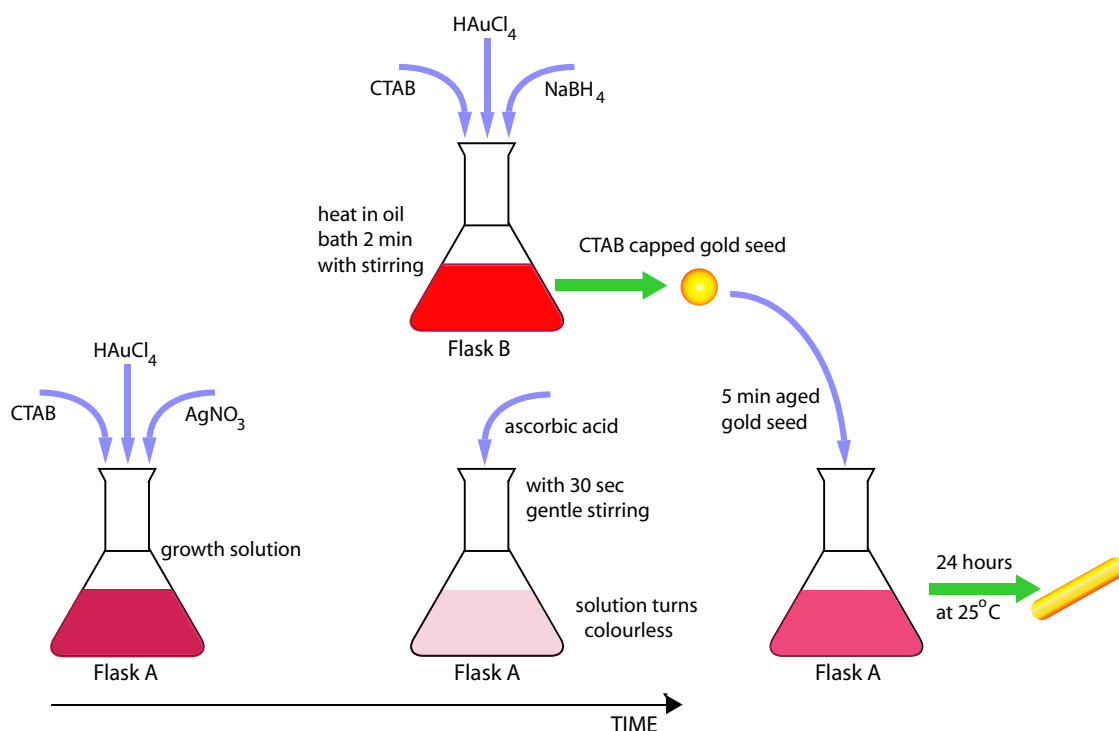


FIG. 2. Schematic of the seed-mediated silver assisted protocol for synthesizing gold nanorods. See text for details.

We used gold salt (Tetrachloroauric acid  $\text{HAuCl}_4 \cdot 3\text{H}_2\text{O}$ , 99.99%) from Acros Organics (Belgium), sodium borohydride ( $\text{NaBH}_4$ , 99%), and ascorbic acid (99%) from Aldrich (The

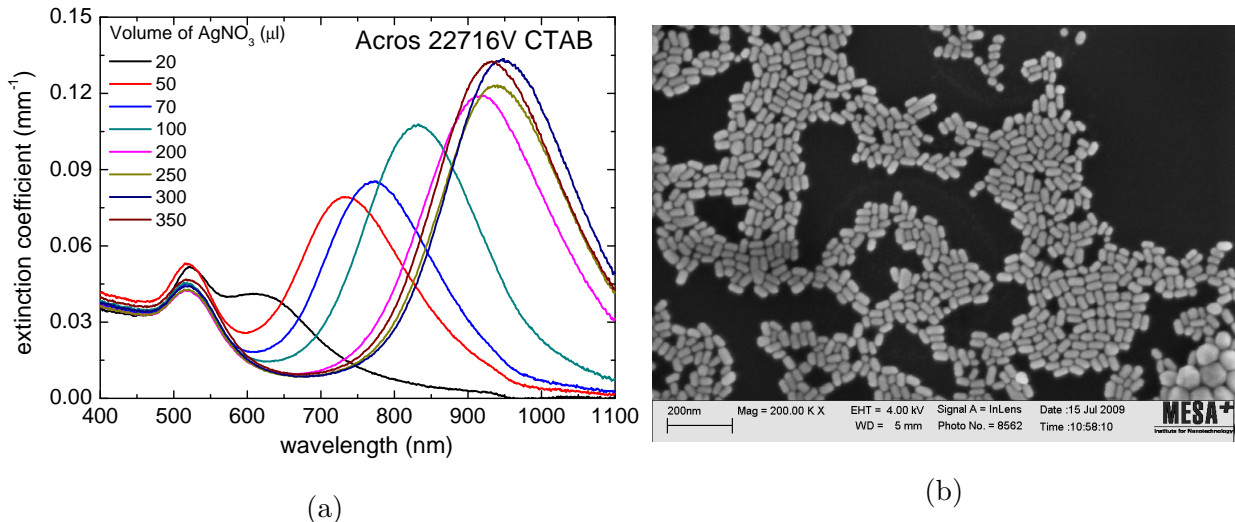


FIG. 3. (a) Optical extinction spectra of AuNR synthesized using various  $\text{Ag}^+$  concentrations in the growth solutions. Signature transverse plasmon (TP) peaks are seen around 516 nm. Red-shifted longitudinal plasmon (LP) peaks in each spectrum indicate the presence of AuNR. (b) A scanning electron micrograph (SEM) of AuNR for the case when 50  $\mu\text{l}$  of 0.01 M  $\text{AgNO}_3$  was used. (Reprinted from Ref [47] with permissions from the authors and the American Chemical Society, copyright 2010 .)

Netherlands), silver nitrate ( $\text{AgNO}_3$ , 99.8%) from Merck (Germany). The CTAB used was product Acros 22716V. Excellent AuNR samples are obtained as witnessed in signature LP peaks in optical extinction spectra, these peaks spanning the spectral range of interest in biomedical imaging (Fig. 3(a)). The SEM image of particles synthesized when 50  $\mu\text{l}$  of  $\text{AgNO}_3$  are used is shown in Fig. 3(b).

The success of the above procedure depends upon several factors including the use of clean glassware and stirrers. We studied the effect of various methods of cleaning glassware. The simplest method was the use of a laboratory steam dishwasher followed by 3 rinsing steps using deionized water. Reasonably high yields of AuNR were synthesized with reproducible LP peaks at the designed wavelengths when the glassware was relatively new. However for best results with highest yields and excellent reproducibility we recommend that all glassware be rinsed with hydrofluoric acid (HF), further with aqua regia ( $\text{HCl}/\text{HNO}_3$ ) and rinsed thoroughly with deionized water prior to use.

Only Milli-Q Gradient System water (Millipore, Bedford, MA, USA) is used for preparing solutions. We prepare the CTAB solution by progressive addition of the flakes to Milli-Q

water maintained at around 45°C in an ultrasonic bath. Gold salt and borohydride solutions need to be freshly prepared, and the latter should be kept ice cold till required.

The chemicals used are crucial for the success of the protocol. Smith and Korgel [46, 48] showed that it was not possible to synthesize AuNR using CTAB products from certain suppliers, which they found to contain iodide impurities. We showed[47] that even within a certain CTAB product, iodide impurities can vary significantly from lot to lot. It should not be a forgone conclusion that AuNR can or cannot be synthesized using certain CTAB products just based upon supplier name and product number; a lot number is required to make such judgements.

One should be aware that it is not possible to exclude variations in environmental conditions such as in ambient temperature etc., uncertainties in experimental conditions such as in seed aging times, component concentrations etc., which could affect in complex ways various steps in the trajectory followed for making AuNR. Thus, if the above protocol fails to produce AuNR, before one changes the CTAB product for another, we recommend that one resort to tweaking concentrations of various products added (starting with AgNO<sub>3</sub>) or fine-tune certain experimental conditions.

### III. OPTICAL CHARACTERIZATION OF GOLD NANORODS

An accurate estimation of the optical absorption coefficient spectrum ( $\mu_a(\lambda)$ ) is important to feedback the synthesis procedure regarding suitability of LP wavelength and the concentrations of NRs ( $N_d$ ) produced. Further, the photoacoustic response following optical absorption is dependent on the  $N$  and their  $\mu_a$ . Knowledge of these two parameters will help in moving towards predicting response, though this response will be heavily modulated by the optical properties of surrounding tissue which will determine the number of photons that will be available for absorption.

Conventional spectroscopy in a vis-NIR photospectrometer is the choice for determining optical properties by measuring collimated transmission spectrum and applying the Beer-Lambert law to calculate the extinction coefficient ( $\mu_e$ ):

$$\mu_e = -\frac{1}{d} \ln \left[ \frac{I}{I_0} \right] \quad (2)$$

where  $d$  is the cuvette length,  $I/I_0$  is the transmitted light intensity.

This approach is suitable to ascertain the position of the LP peak. However, determining  $\mu_a$  from the measurement is not straightforward since most particles considered for photoacoustics have their largest dimension greater than 50 nm, when their scattering coefficient  $\mu_s$  becomes non-negligible.

The following approach is usually adopted: the average size of the particles is ascertained using electron microscopy (EM). With the value of dielectric function of gold and that of the embedding material (water), the optical interaction efficiencies ( $Q_e, Q_a, Q_s$ ) are calculated using numerical methods such as the Discrete Dipole Approximation (DDA) [49]. Knowing the geometrical cross-sections, the interaction cross-sections ( $\sigma_e, \sigma_a, \sigma_s$ ) can be calculated.

Under the assumption that the particles are clones of the simulated particle, the number density ( $N_d$ ) of the particles is calculated from the extinction coefficient ( $\mu_e$ ) as:

$$N_d = \frac{\mu_e}{\sigma_e} \quad (3)$$

Absorption/scattering coefficients are now calculated as:

$$\mu_{a/s} = N_d \times \sigma_{a/s} \quad (4)$$

This method has the drawback that in the literature for the popular implementation of the DDA method there are inconsistencies in the choice of various parameters required for the simulations which lead to considerable inaccuracies in the results. We provide a critical discussion of the most important input required for accurate modelling.

### A. DDA simulations of optical properties

DDSCAT 6.1 [50] is a FORTRAN package that implements the DDA method to simulate interaction of electromagnetic radiation with particles of arbitrary shape and composition. The particle is subdivided into  $N$  polarizable points, located on a cubic lattice with an interdipole distance  $d$  given by  $V = Nd^3$  where  $V$  is the volume of the particle. The radiation scattered and absorbed by the target is computed taking into consideration dipole-dipole interactions.

The output parameters from the simulation are extinction, absorption and scattering efficiencies ( $Q_e, Q_a, Q_s$ ) which yield the corresponding cross-sections of the particle when multiplied by  $\pi r_{eff}^2$ . The effective radius  $r_{eff}$  is the radius of a sphere having a volume equal to that of the particle and is given by  $(3V/4\pi)^{1/3}$ .

As mentioned earlier, no universal agreement exists on a number of parameters in the use of DDSCAT such as the number of dipoles chosen for discretization, on the shape used to represent the nanorods and on the dielectric function of gold required for the simulations. In Ref. [51] we systematically studied the influence of these parameters on simulated results, but here we will discuss only the choice of dielectric function which is of great importance in the simulations. Prior reports used without justification experimental data tabulated by either Johnson and Christy [52], Palik [53] or Weaver [54]. Further, sometimes bulk values and at other times size corrections modifications to account for surface damping have been used. With all other parameters remaining the same, a wide spread in the position of the LP maximum is obtained for the different sources for the dielectric function. We found that there is reasonable consistency between our experiments and simulation with the use of size-corrected data from Palik [53], which could be the best choice for the dielectric function. The dielectric function of gold from Palik [53] was determined under ultrahigh vacuum conditions which suggests reliability. However, much still needs to be learnt regarding the dielectric function of gold at the nanoscale.

## B. Experimental quantitation of optical properties

We have shown that it is not possible to objectively compare experimental data with the simulations owing to the various input parameters, such as the shape (not discussed here) used to represent the NRs and the dielectric function of gold. Consequently, the value estimated for  $\sigma_e$  can be inaccurate; the errors propagating in subsequent calculation steps to the values of absorption  $\mu_a$  and scattering  $\mu_s$  coefficients.

Currently, only a few experimental techniques have been reported against the backdrop of the limitations of the conventional approach. The photoacoustic method [55] is the most robust since it measures  $\mu_a$  directly as a driver of the ultrasound detected. The method requires a previous calibration of the system against an absorber whose  $\sigma_a$  is known.

Recently we presented a novel approach to determine the ensemble optical properties (both  $\mu_a$  and  $\mu_s$ ) of AuNR [56]. This method is based on a dual-fiber approach called differential pathlength spectroscopy (DPS) [57, 58]. One fiber delivers and collects ( $dc$ ) photons from the sample, the second fiber adjacent to the first, only collects ( $c$ ) photons. A schematic of the setup is shown in Fig. 3; details are provided in Ref. [56]. When the photon

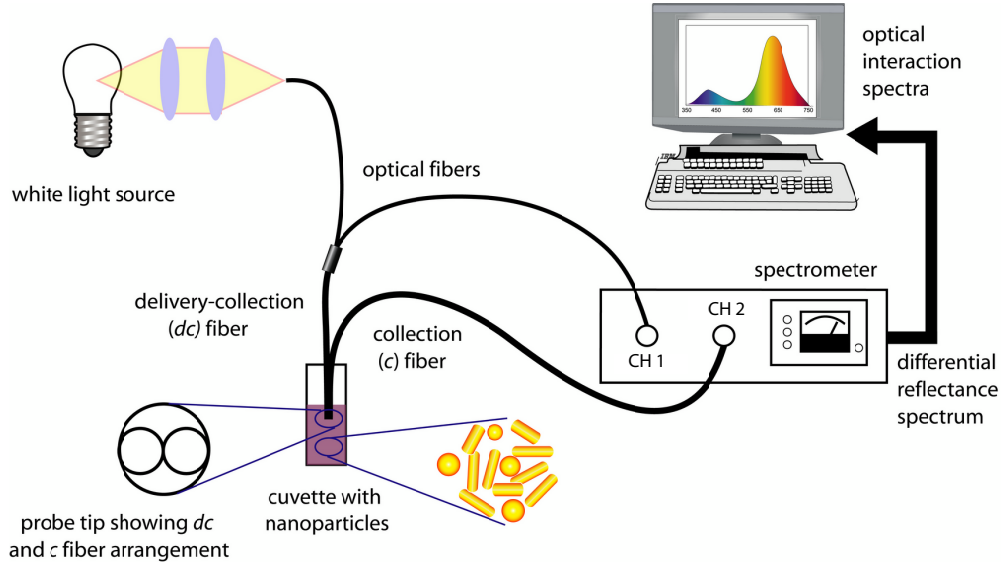


FIG. 4. Differential pathlength spectroscopy (DPS) experimental setup for determining the optical properties of small volumes of gold nanorods. (Reprinted from Ref [56] with permissions from the authors and the American Chemical Society, copyright 2010.)

mean free path is smaller than the fiber diameter, the differential reflectance  $\mathbf{R}$ , obtained by subtracting the  $c$  signal from the  $dc$  signal originates from a constant apparent pathlength. This term, called the differential pathlength [57, 58], depends only upon the fiber diameter, so that its knowledge allows quantitative determination of the optical properties in highly scattering media.

When a fiber of small numerical aperture (say N. A. = 0.22) is used, the backscattering signal is given by [56]:

$$\mathbf{R}_{\text{sing}} = C_{\text{app}} \mu_{\text{bk}} \quad (5)$$

where  $C_{\text{app}}$  is an instrument constant and  $\mu_{\text{bk}}$  the backscattering coefficient. This  $\mu_{\text{bk}}$  is given by:

$$\mathbf{R}_{\text{sing}} = C_{\text{app}} \mathbf{p}(180) \mu_s \quad (6)$$

where  $\mathbf{p}(180)$  is the phase function of scattering sampled at  $180^\circ$ . To determine  $C_{\text{app}}$  above, the DPS system requires calibration against a medium with well-characterized optical properties such as NIST certified polystyrene beads. Thus, from eq 6, it is clear that the acquired DPS signal can be related to  $\mu_s$ .

To convert this to the scattering coefficient ( $\mu_s$ ), a theoretical calculation of the phase function at  $180^\circ$  of the particles is required. We resorted to DDSCAT simulations, but we

showed that this  $\mathbf{p}(180)$  is only marginally susceptible to error [56]. This is in sharp contrast to the inaccuracies in calculated interaction efficiencies ( $Q$ 's) as discussed above. Finally, using the extinction coefficient ( $\mu_e$ ) obtained using a standard UV-vis-NIR photospectrometer measurement,  $\mu_a$  is easily obtained.

#### IV. BIOCOMPATIBILITY OF GOLD NANORODS BY PEG COATING

The surfactant CTAB is crucial for the synthesis of rod-shaped nanoparticles. CTAB (and silver) stabilize the  $\{110\}$  faces of gold seed to a greater extent than the  $\{100\}$  surfaces leading to a faster rate of gold atom deposition on the latter, leading to one-dimensional growth along the  $[100]$  direction [40–42]. The CTAB bilayer [59] also helps preserve colloidal stability by electrostatic repulsion due to its a nett positive charge on the particle surface. CTAB is thus indispensable for preparing highly monodisperse and stable particles with controllable aspect ratios [38, 60].

However, CTAB disrupts cell-membrane integrity [61] and is severely toxic. Such CTAB-AuNR intended for any biomedical applications need to be detoxified by removing excess unbound CTAB from the dispersing medium by centrifugation. This process however also strips stabilizing CTAB off the gold, which increases the tendency of the particles to aggregate. It is also possible that CTAB molecules can desorb from the gold surfaces, making the particles potentially toxic.

An excellent approach to ensure biocompatibility is to PEGylate NRs, which has been shown to ameliorate cell toxicity in several cell lines [62–65], by largely replacing CTAB. We expanded the cell-toxicity studies by applying PEGylated nanorods to a number of cell lines: SKBR3, CHO, C2C12 and HL60 cells [66].

The following is the procedure that we follow [66]: The stock solution is centrifuged at 10000 G for 20 minutes, and the pellet redispersed in water. The centrifugation step is repeated a second time, with the resulting NR pellet now dispersed in 0.5 ml of 5 mM mPEG-SH with vigorous vortexing for 20 seconds. To this, 0.5 ml of 1X PBS (Phosphate Buffer Saline) is added followed by continuous rotation for 24 hours at 4°C. The resultant is subjected to two centrifugation steps to remove excess mPEG-SH from the solution and the pellet dispersed in 2.5 ml 1X PBS.

The result is strong sulphur binding of the SH terminal of mPEG-SH to the gold surface,

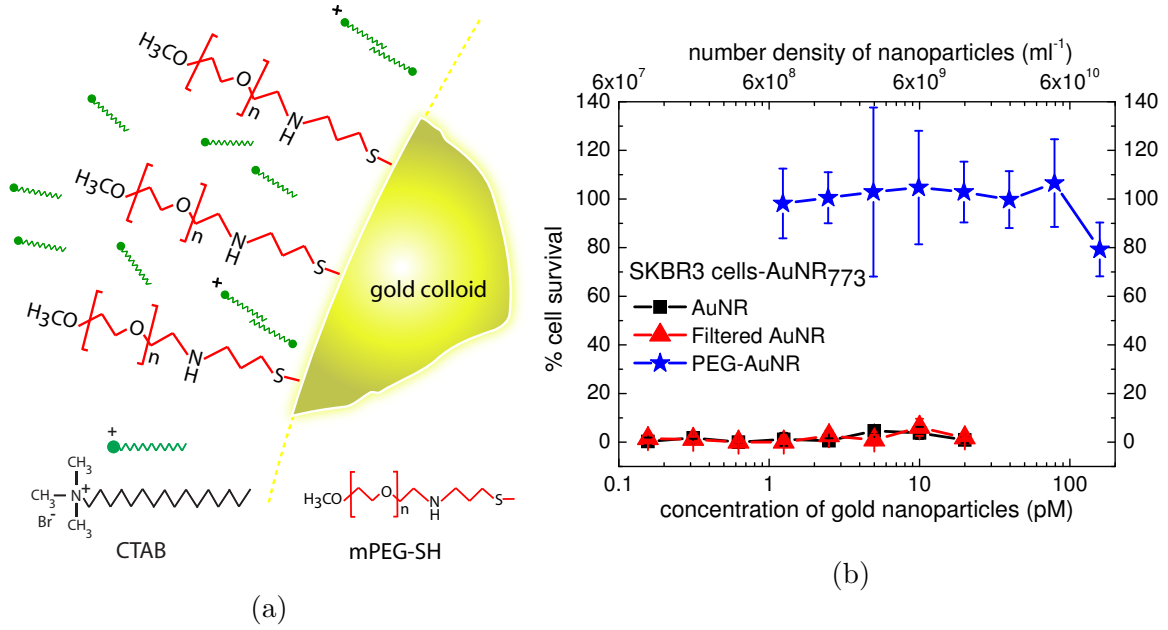


FIG. 5. (a) Model for surface modification of gold nanorods using mPEG-SH, where sulphur-gold binding ensures replacement of the CTAB bilayer by PEG. (b) Dose-response curves of the SKBR3 cell-line following exposure to various gold nanorods having longitudinal plasmon peak at 773 nm. Particles studied are AuNR773, filtered AuNR773, PEGylated AuNR773 and PSS-treated AuNR773. (Adapted from Ref [66] with permissions from the authors and the Institute of Physics (IOP) Publishing, copyright 2010.)

with replacement of (most of) the CTAB bilayer. A model of the resultant is shown in Fig. 5(a). Evidence for this can be obtained by measuring zeta-potential values [66] for the resultant. Neutral to near-neutral values indicate PEG replacement of most of the positively charged CTAB. In such a case there will be no compromise in colloidal stability, since the completely formed PEG layer takes over the stabilizing role of CTAB, but with a steric hindrance mechanism compared with CTAB's electrostatic or charge stabilization. The optical spectra of the particles before and after PEGylation should be measured to verify that the characteristic plasmon peaks are preserved and that the colloid is stable. We have found that the particles processed in this way with PEG, retain excellent dispersion stability even after mixing in cell culture media [66].

We found that the PEGylated particles elicited excellent cell viability and were essentially non-toxic for the SKBR3, CHO and C2C12 cell-lines up to concentrations of 165 pm corresponding to approximately  $1 \times 10^{11}$  NR/ml. Typical dose response curves using

products from batch AuNR<sub>773</sub> (AuNR with LP peak at 773 nm) on the SKBR3 cell-line is shown in Fig. 4(b). Further, we found from TEM that PEG-AuNR were absent inside SKBR3 cells [66] after 3 hours of exposure. In combination with the low toxicity profile this indicated that PEG-AuNRs have little interaction with cells.

Next we tested the particles *in vivo* with all the complexity of blood flow, immunological and inflammatory responses. Specifically we compared the blood clearance and tissue distribution of CTAB-capped and PEG-coated AuNR after intravenous injection in the tail vein of rats [67]. The gold content in blood and various organs was measured quantitatively with inductively coupled plasma mass spectrometry (ICP-MS).

The CTAB capped gold nanorods were almost immediately ( $< 15$  minutes) cleared from the blood circulation whereas the PEG-AuNR resulted in a prolonged blood circulation with a half lifetime ( $t_{1/2}$ ) of 19 h [67] (Fig. 5(a)). We surmised that with CTAB-AuNR, a serum protein ‘corona’ [68–70] comprising opsonin ligands, is immediately formed. This would initiate mechanisms of recognition and internalization by components of the reticuloendothelial system (RES). Rapid clearance of the CTAB-AuNR from blood would follow, with their deposition into organs of the RES.

On the other hand, the hydrophilic and neutral PEG coating prevents or minimizes adsorption of serum proteins on the AuNR [71, 72] Further close approach of the underlying AuNR to cell surfaces is precluded by the PEG layer [71, 72]. The effect is thus minimal interaction of the AuNR with macrophage cell receptors: PEG-AuNRs thus experience prolonged blood persistence (see also Fig. 5(b)).

In addition to the dramatic differences in blood clearance kinetics between the two types of particles, the final organ distribution of the particles was also significantly different. CTAB-AuNR were taken up predominantly by the liver, and to a lesser extent by the spleen followed by the lungs. On the other hand, the PEG-coating served to shift the distribution profile more towards the spleen with a 6 day dose per gram organ 6.8 times in excess of that in the liver, as depicted in Fig. 5(c).

Thus, PEGylation of AuNRs resulted in a prolongation of the blood clearance (up to 48 hours) and the highest organ exposure in the spleen. In view of the time frame of the observed presence in blood circulation, PEG-AuNR can be considered to be promising candidates for *in vivo* use.

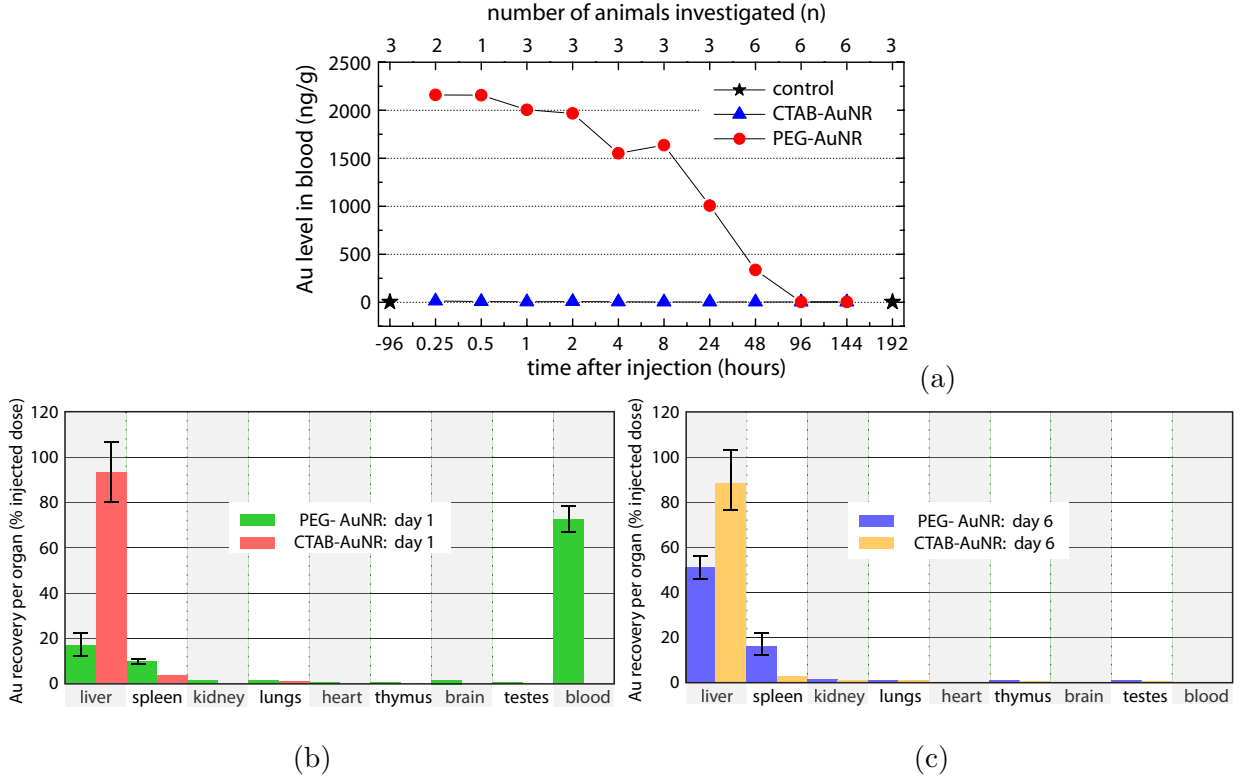


FIG. 6. (a) Blood clearance of PEGylated (PEG-AuNR) and non-PEGylated (CTAB-AuNR) gold nanorods. (b) Recovery of gold from various harvested organs as percentage of administered dose for PEG-AuNR and CTAB-AuNR on day 1, and (c) on day 6.

## V. BIONJUGATION OF GOLD NANORODS WITH ANTIBODIES

There are broadly two methods of coupling AuNRs with affinity biomolecules: using non-covalent means [10, 73] and covalent means [74, 75].

### A. Non-covalent conjugation of the antibody to colloidal gold

This method relies on the existence of negative charge on the particles' surface which attracts positively charged amino groups of the antibody. When the protein comes close enough for binding, the hydrophobic pockets of the protein will make contact and bind with the gold.

In general, for optimum conjugation, it is recommended that the pH of the mAB and gold sol be maintained at or slightly higher than the isoelectric point (pI) of the antibody [76]. The minimum protecting amount of mAB is incubated with the AuNR for conjugation to

take place. The minimum protecting amount of protein is that amount that is required to maintain colloidal stability of the conjugated NPs upon addition of NaCl [76] as judged by colorimetric analysis. To block the free surfaces on the gold 10 % Bovine Serum Albumin (BSA) maintained at the same pH as the antibody solution, is added to the resultant.

Using this method, we conjugated gold nanospheres (AuNS) and AuNRs with HER81 antibody, which bind with high efficiency to HER81 receptors expressed by SKBR3 breast carcinoma cells [10]. Citrate capped AuNS are negatively charged due to a layer of negative citrate ions and are well suited to the method described. With AuNR the situation is more complex: their sidewalls are stabilized with a CTAB bilayer, which imparts a positive charge to the surface. We surmised that in spite of the net positive charge, the unpassivated end faces would be negatively charged due to the presence of  $\text{AuCl}^{-2}$  ions [77]. We therefore followed the same protocol and performed immunostaining studies using the SKBR3 cell-line, which demonstrated the success of the bioconjugation and the retention of the functionality of the mAB.

## B. Covalent binding of antibodies to gold nanorods

The method of non-covalent binding is expected to be less strong and less stable especially in the hostile environments found *in vivo*, and covalent binding is used. As the name suggests, a linker couples the antibody to the gold surface using covalent coupling. Huff *et al* [65] used a heterobifunctional cross-linker LC-SPDP to connect antibodies to the AuNR surface using the covalent binding of the pyridildithio group to gold. Recently, Eghtedari *et al* [78] reported the use of nanothinks acid activated by EDC-NHS to couple antibodies covalently to AuNR.

We used a heterobifunctional PEG linker (OPSS-PEG-NHS) to achieve covalent coupling of HER81 antibodies to AuNRs. This strategy was inspired by the work of Loo *et al* [75] who used the approach to couple gold nanoshells to HER2 antibody. Figure 6 depicts the procedure. The following are the steps followed:

1. **Coupling of OPSS-PEG-NHS to HER81 mAb** The PEG linker is made to couple to the HER81 via amide bonding via the linker's NHS group. The linker is dispersed in  $\text{NaHCO}_3$  (100mM, pH 8.5) and 81  $\mu\text{mol/L}$  (0.13 mg/ml) of the resultant is mixed with 5.4  $\mu\text{mol/L}$  (1 mg/ml) HER81 mAb at a volumetric ratio of 1:9. The HER81-

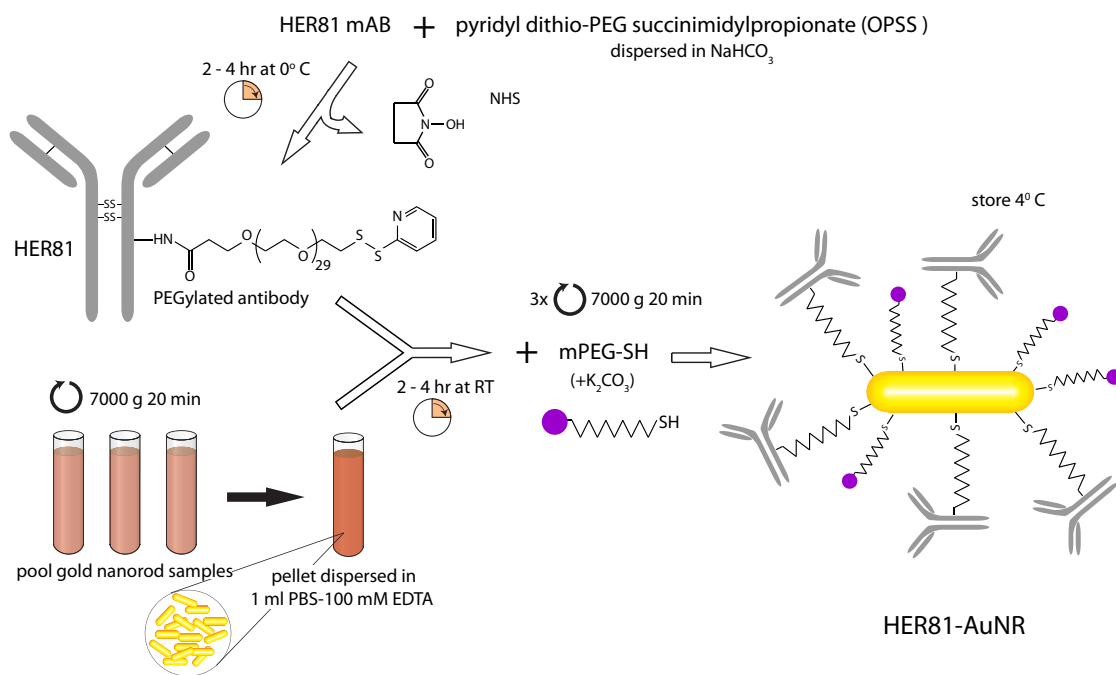


FIG. 7. Schematic representation of the procedure of covalently coupling the HER81 mAb to the gold nanorods using a heterobifunctional PEG linker OPSS.

OPSS-PEG-NHS is incubated on ice. The PEGylated mAb is dialyzed (MW=7,000) to remove excess linker; PBS is used as dialysis buffer. The samples are stored at  $4^\circ\text{C}$ .

- Coupling of PEG-linker-HER81 to gold nanorods** Two ml of AuNR are centrifuged at 7000 g/20 minutes in a low-binding micro tube. The pellets from several samples are added to increase the concentration. The AuNR are dispersed in 1 ml PBS with 100 mM EDTA with gentle mixing.

The PEG-linker-HER81 is added with vortexing to the AuNR and allowed to stand for two hours. After incubation,  $100\ \mu\text{l}$  of 2 mM  $\text{K}_2\text{CO}_3$  and  $12\ \mu\text{l}$  of 5 mM mPEG-SH is added. The resultant is rotated overnight at room temperature (RT); then centrifuged three times at 7000 g/20 minutes. The pellet is dispersed in 1X PBS and stored at  $4^\circ\text{C}$ .

The biconjugation was a success as borne out from confocal microscopy visualizations of immunostaining studies using the SKBR3 breast adenocarcinoma cell-line. The protocol appeared to be robust and dependable for bioconjugation and the functionality of the product

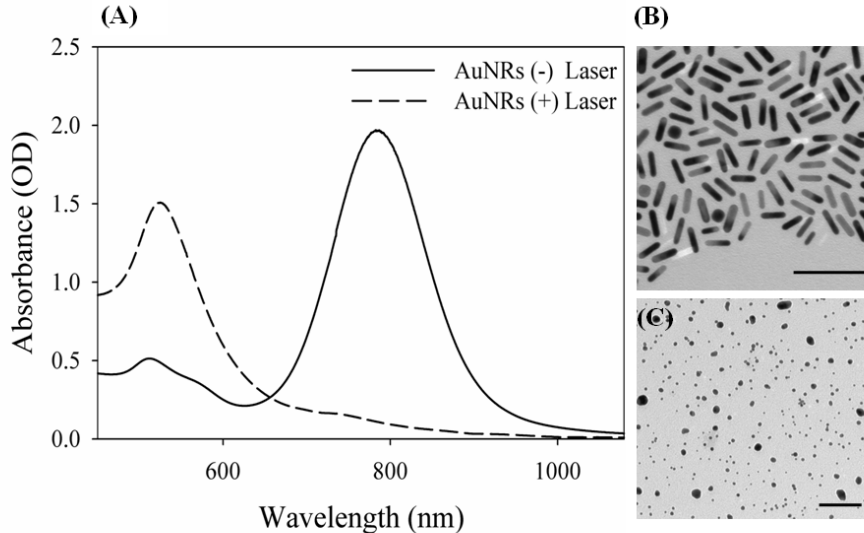


FIG. 8. (A) Absorbance spectra showing the longitudinal plasmon (LP) peak of gold nanrods (AuNR) before (solid line) and after (dashed line) pulsed laser irradiation using 1000 pulses at  $120 \text{ mJc m}^{-2}$  at 800 nm. Transmission electron micrographs (TEM) of the AuNR before (B), and after (C) laser exposure. The AuNR are deformed into spherical particles. (Reproduced from Ref. [81] with permission from the authors and the Institute of Physics (IOP) Publishing, copyright 2009.)

was stable to well after 6 months.

## VI. PULSED LIGHT INTERACTIONS WITH GOLD NANORODS

The thermodynamic tendency to lower surface energy would imply that nanorods are unstable with respect to nanospheres. Pioneering investigations by Chang *et al*[79] and Link *et al*[80] independently demonstrated that illumination of AuNR with high fluences of pulsed laser light at the LP peaks caused shape transformation towards the thermodynamically favorable spherical shape. Thermal equilibration between electrons and the lattice in electron-phonon coupling was thought to cause temperatures in excess of melting to cause the structural rearrangements[5]. At fluences lower than a certain not-well defined threshold sometimes intermediate forms with lower aspect ratios than the original were also observed. The effect of this shape transformation on the optical properties was spectacular: with sufficient numbers of high intensity laser pulses at the LP peak ensemble populations of AuNR would form spheres, causing the LP to disappear with an accompanying increase in the TP peak (See Fig. 6). The implication of this LP bleaching from an imaging point of view is a

loss of contrast at the NIR wavelength of interest. Didychuk *et al*[81] experimentally studied the photon-driven AuNR reshaping phenomenon in tissue phantoms dispersed with AuNR, using ns laser pulses at the LP wavelength, in a combination of energies and pulse counts. Their most important finding was that at the maximum permissible exposure (MPE) 30 mJ cm<sup>-2</sup>, for the specifications of the laser used, NR conversion to spheres occurred to a depth of 6 mm after 100 pulses. The implication for PA imaging is that at the MPE, the use of AuNR for contrast applications is not applicable for depths less than 6-10 mm. For deeper lying target sites the illuminated particles maintain their morphologies preserving the necessary sharp absorption peaks at the designed wavelength.

Recent work from the groups of P.-C. Li [82] and Emenialov [83] has shown that the threshold for photon-induced reshaping can be raised by encapsulating AuNR in an amorphous silica matrix. Both groups use a single-step method where an alkoxide-based silica precursor, tetraethyl orthosilicate (TEOS), is added to the rods at a pH that is adjusted to around 11. With time, mesoporous silica coatings are uniformly deposited on the AuNRs. It has been hypothesized by Gorelikov and Matsuura[84], that CTAB molecules on the AuNR serve as the organic template for the formation of the mesoporous silica coating via base-catalyzed hydrolysis of TEOS and subsequent condensation of silica onto the surface of the CTAB molecules. The effect of the silica coating is to improve the stability of the AuNR due to its mechanical rigidity, while not influencing the optical properties due to its transparency at NIR wavelengths. Indeed, studies have shown that the silica-coated AuNR retained their morphologies to upto 3 times higher fluences than bare AuNR[83].

## VII. CONCLUDING REMARKS

As we show, AuNR possess vast potential in enhancing the application of PA imaging due to their plasmon resonance-driven optical absorptions at the red and NIR wavelengths. Pre-clinical studies on mice and rats have convincingly demonstrated that the sensitivity of PA imaging and specificity to the disease are improved by using appropriately targeted AuNR. The use of these NRs for these applications is set to intensify as great strides are being made in the technology relating to PA instrumentation, while new NR synthetic protocols are becoming available and new disease targets are being pursued with the use of affinity molecules such as antibodies and ligands. While much has been learnt from

the initial use of AuNR, there are many gaps in our understanding of behavior at the nanoscale especially in synthesis of the particles and their interactions with living media. A better understanding of the underlying mechanisms of synthesis will provide a handle toward the desired reproducible control over AuNR sizes and shapes, that will accelerate the transition of certain synthetic routes from laboratory protocols to manufacturing processes. For the application of AuNR to move into the crucial phase of clinical trials a complete understanding of particle interactions with various biological specimens is required. While detoxification is at the moment performed downstream of synthetic protocols which employ toxic components, it is imperative that non-toxic green chemicals be used for synthesis. At this moment, not much research has been conducted in this regard. In addition for *in vivo* use, there exist several biological and biophysical challenges presented to AuNR (and other nanoparticles) in reaching the targeted site following administration into the body. The particles need to extravasate the vascular compartment, avoid uptake by organs of the reticuloendothelial system, penetrate through the interstitium, bind to and be taken-up by the target cells. Much work is still required to overcome the barriers, but these challenges are similar to those faced in conventional drug delivery where there is more experience with several creative solutions being researched, which will help the AuNR delivery problem.

## VIII. ACKNOWLEDGEMENTS

We acknowledge the contributions of colleagues Dr. Raja Gopal Rayavarapu and Ms. Wilma Petersen in the work described. We are also grateful to our collaborators Dr. Wim de Jong (RIVM), Dr. Fijs van Leeuwen (NKI), Dr. Cees Otto, Ms. Liesbeth Hartsuiker, Prof. Leon Terstappen, Dr. Arjen Amelink (EMC) and Prof. Dick Sterenberg (EMC).

Prof. Pai-Chi Li, Dr. Daniel Razansky, Ms. Candice Didychuk and Dr. Jeffrey Carson are thanked permissions to reprint and for providing original figures.

The work was funded through the thrust area program NIMTIK of the University of Twente; through the PRESMITT project (IPD067771) of the AgentschapNL program IOP Photonic Devices; and by the Nederlandse Wetenschappelijk Organisatie (NWO) and Sticht-

ing Technische Wetenschappen (STW) through project TTF 6527.

---

- [1] K. L. Kelly, E. Coronado, L. L. Zhao, and G. C. Schatz, *The Journal of Physical Chemistry B*, **107**, 668 (2003).
- [2] F. Wagner, S. Haslbeck, L. Stievano, S. Calogero, Q. Pankhurst, and K.-P. Martinek, *Nature*, **407**, 691 (2000).
- [3] P. Edwards and J. Thomas, *Angewandte Chemie - International Edition*, **46**, 5480 (2007).
- [4] H. Horvath, *Journal of Quantitative Spectroscopy and Radiative Transfer*, **110**, 787 (2009).
- [5] S. Link and M. El-Sayed, *International Reviews in Physical Chemistry*, **19**, 409 (2000).
- [6] C. Bohren and D. Huffman, *Absorption and scattering of light by small particles*, edited by U. Wiley Science Paperback Series, Chichester (Cambridge University Press, New York, NY, USA, 1998).
- [7] R. E. Hummel, "Electronic properties of materials," (Springer-Verlag, Berlin, 1993) Chap. 13, p. 225, 2nd ed.
- [8] J. Perez-Juste, I. Pastoriza-Santosa, L. M. Liz-Marzn, and P. Mulvaney, *Coord. Chem. Rev.*, **249**, 1870 (2005).
- [9] C. J. Murphy, T. K. Sau, A. M. Gole, C. J. Orendorff, J. Gao, L. Gou, S. E. Hunyadi, and T. Li, *J. Phys. Chem. B*, **109**, 13857 (2005).
- [10] R. Rayavarapu, W. Petersen, C. Ungureanu, J. Post, T. van Leeuwen, and S. Manohar, *Int. J. Biomed. Imaging*, **29817**, 29817 (2007).
- [11] R. R. Kortom and E. Sevick-Muraca, *Annu. Rev. Phys. Chem*, **47**, 555 (1996).
- [12] B. J. Tromberg, N. Shah, R. Lanning, A. Cerussi, J. Espinoza, T. Pham, L. Svaasand, and J. Butler, *Neoplasia*, **2**, 2640 (2000).
- [13] A. Oraevsky, A. Karabutov, and E. Savateeva, *Proc. SPIE*, **4434**, 60 (2001).
- [14] J. Copland, M. Eghtedari, V. Popov, N. Kotov, N. Mamedova, M. Motamedi, and A. Oraevsky, *Molecular Imaging and Biology*, **6**, 341 (2004).
- [15] P.-C. Li, S.-W. Huang, C.-W. Wei, Y.-C. Chiou, C.-D. Chen, and C.-R. Wang, *Optics Letters*, **30**, 3341 (2005).
- [16] V. Zharov, E. Galanzha, E. Shashkov, N. Khlebtsov, and V. Tuchin, *Optics Letters*, **31**, 3623 (2006).

- [17] C.-W. Wei, S.-W. Huang, C.-R. Wang, and P.-C. Li, *IEEE Transactions on Ultrasonics, Ferroelectrics, and Frequency Control*, **54**, 1131 (2007).
- [18] K. Kim, S.-W. Huang, S. Ashkenazi, M. O'Donnell, A. Agarwal, N. Kotov, M. Denny, and M. Kaplan, *Applied Physics Letters*, **90** (2007).
- [19] M. Eghtedari, A. Oraevsky, J. Copland, N. Kotov, A. Conjusteau, and M. Motamedi, *Nano Letters*, **7**, 1914 (2007).
- [20] P.-C. Li, C.-W. Wei, C.-K. Liao, C.-D. Chen, K.-C. Pao, C.-R. Wang, Y.-N. Wu, and D.-B. Shieh, *IEEE Transactions on Ultrasonics, Ferroelectrics, and Frequency Control*, **54**, 1642 (2007).
- [21] A. Agarwal, S. Huang, M. O'Donnell, K. Day, M. Day, N. Kotov, and S. Ashkenazi, *Journal of Applied Physics*, **102** (2007).
- [22] D. Chamberland, A. Agarwal, N. Kotov, J. Brian Fowlkes, P. Carson, and X. Wang, *Nanotechnology*, **19** (2008).
- [23] P.-C. Li, C.-R. Wang, D.-B. Shieh, C.-W. Wei, C.-K. Liao, C. Poe, S. Jhan, A.-A. Ding, and Y.-N. Wu, *Optics Express*, **16**, 18605 (2008).
- [24] K. Song, C. Kim, K. Maslov, and L. Wang, *European Journal of Radiology*, **70**, 227 (2009).
- [25] S. Mallidi, T. Larson, J. Tam, P. Joshi, A. Karpouk, K. Sokolov, and S. Emelianov, *Nano Letters*, **9**, 2825 (2009).
- [26] A. Taruttis, E. Herzog, D. Razansky, and V. Ntziachristos, *Optics Express*, **18**, 19592 (2010).
- [27] Y. Wang, X. Xie, X. Wang, G. Ku, K. Gill, D. O'Neal, G. Stoica, and L. Wang, *Nano Letters*, **4**, 1689 (2004).
- [28] K. Song, C. Kim, C. Cobley, Y. Xia, and L. Wang, *Nano Letters*, **9**, 183 (2009).
- [29] X. Yang, S. Skrabalak, Z.-Y. Li, Y. Xia, and L. Wang, *Nano Letters*, **7**, 3798 (2007), cited By (since 1996) 54.
- [30] D. Pan, M. Pramanik, A. Senpan, S. Ghosh, A. A. Wickline, L. V. Wang, and G. M. Lanza, *Biomaterials*, **31**, 4088 (2010).
- [31] H. Cui and X. Yang, *Medical Physics*, **37**, 4777 (2010).
- [32] D. Razansky, J. Baeten, and V. Ntziachristos, *Medical Physics*, **36**, 939 (2009).
- [33] X. Yang, E. Stein, S. Ashkenazi, and L. Wang, *Wiley interdisciplinary reviews. Nanomedicine and nanobiotechnology*, **1**, 360 (2009).
- [34] Y.-Y. Yu, S.-S. Chang, C.-L. Lee, and C. Wang, *Journal of Physical Chemistry B*, **101**, 6661

(1997).

- [35] N. R. Jana, L. Gearheart, and C. J. Murphy, *J. Phys. Chem. B*, **105**, 4065 (2001).
- [36] A. Gole and C. J. Murphy, *Chem. Mater.*, **16**, 3633 (2004).
- [37] N. R. Jana, L. Gearheart, and C. J. Murphy, *Adv. Mater.*, **13**, 1389 (2001).
- [38] B. Nikoobakht and M. A. El-Sayed, *Chem. Mater.*, **15**, 1957 (2003).
- [39] Y. Xia, Y. Xiong, B. Lim, and S. E. Skrabalak, *Angew. Chem. Int. Ed.*, **48**, 60 (2009).
- [40] M. Liu and P. Guyot-Sionnest, *J. Phys. Chem. B*, **109**, 22192 (2005).
- [41] C. J. Orendorff and C. J. Murphy, *J. Phys. Chem. B*, **110**, 3990 (2006).
- [42] M. Grzelczak, J. Prez-Juste, P. Mulvaney, and L. M. Liz-Marzán, *Chem. Soc. Rev.*, **37**, 1783 (2008).
- [43] A. V. Alekseeva, V. A. Bogatyrev, L. A. Dykman, B. N. Khlebtsov, L. A. Trachuk, A. G. Melnikov, and N. G. Khlebtsov, *Appl. Opt.*, **44**, 6285 (2005).
- [44] L. Gou and C. J. Murphy, *Chem. Mater.*, **17**, 3668 (2005).
- [45] B. Wang, E. Yantsen, T. Larson, A. Karpiouk, S. Sethuraman, J. Su, K. Sokolov, and S. Emelianov, *Nano Letters*, **9**, 2212 (2009).
- [46] D. K. Smith and B. A. Korgel, *Langmuir*, **24**, 644 (2008).
- [47] R. Rayavarapu, C. Ungureanu, P. Krystek, T. Van Leeuwen, and S. Manohar, *Langmuir*, **26**, 5050 (2010).
- [48] D. K. Smith, N. R. Miller, and B. A. Korgel, *Langmuir*, **25**, 9518 (2009).
- [49] E. M. Purcell and C. R. Pennypacker, *Astrophys. J.*, **186**, 705 (1973).
- [50] B. T. Draine and P. J. Flatau, *Journal of the Optical Society of America A: Optics and Image Science, and Vision*, **11**, 1491 (1994).
- [51] C. Ungureanu, R. G. Rayavarapu, S. Manohar, and T. G. Van Leeuwen, *J. Appl. Phys.*, **105**, 102032 (2009).
- [52] P. Johnson and R. Christy, *Physical Review B*, **6**, 4370 (1972).
- [53] E. D. Palik, *Handbook of optical constants of solids* (Academic Press, New York, 1985).
- [54] J. Weaver, C. Krafka, D. Lynch, and E. Koch, *Noble Metals, Aluminium, Scandium, Yttrium, the Lanthanides and the Actinides*, *Handbook of optical constants of solids*, Vol. 2 (Fach-Informationen Zentrum, Karlsruhe, 1981).
- [55] E. Cho, C. Kim, F. Zhou, C. Cobley, K. Song, J. Chen, Z.-Y. Li, L. Wang, and Y. Xia, *Journal of Physical Chemistry C*, **113**, 9023 (2009).

- [56] C. Ungureanu, A. Amelink, R. Rayavarapu, H. Sterenborg, S. Manohar, and T. Van Leeuwen, *ACS Nano*, **4**, 4081 (2010).
- [57] A. Amelink, M. P. L. Bard, S. A. Burgers, and H. J. C. M. Sterenborg, *Appl. Opt.*, **42**, 4095 (2003).
- [58] A. Amelink and H. J. C. M. Sterenborg, *Appl. Opt.*, **43**, 3048 (2004).
- [59] B. Nikoobakht and M. A. El-Sayed, *Langmuir*, **17**, 6368 (2001).
- [60] J. Gao, C. M. Bender, and C. J. Murphy, *Langmuir*, **19**, 9065 (2003).
- [61] A. P. Leonov, J. Zheng, J. D. Clogston, S. T. Stern, A. K. Patri, and A. Wei, *ACS Nano*, **2**, 2481 (2008).
- [62] N. Lewinski, V. Colvin, and R. Drezek, *Small*, **4**, 26 (2008).
- [63] T. Nidome, M. Yamagata, Y. Okamoto, Y. Akiyama, H. Takahashi, T. Kawano, Y. Katayama, and Y. Niidome, *J. Contl. Release*, **114**, 343 (2006).
- [64] H. Takahashi, Y. Niidome, T. Niidome, K. Kaneko, H. Kawasaki, and S. Yamada, *Langmuir*, **22**, 2 (2006).
- [65] T. B. Huff, M. N. Hansen, Y. Zhao, J.-X. Cheng, and A. Wei, *Langmuir*, **23**, 1596 (2007).
- [66] R. Rayavarapu, W. Petersen, L. Hartsuiker, P. Chin, H. Janssen, F. Van Leeuwen, C. Otto, S. Manohar, and T. Van Leeuwen, *Nanotechnology*, **21** (2010).
- [67] D. Lankveld, R. Rayavarapu, P. Krystec, A. G. Oomen, H. W. Verharen, T. G. van Leeuwen, W. de Jong, and S. Manohar, *Nanomedicine*, **6**, in print (2011).
- [68] M. Dobrovolskaia, A. Patri, J. Zheng, J. Clogston, N. Ayub, P. Aggarwal, B. Neun, J. Hall, and S. McNeil, *Nanomedicine: Nanotechnology, Biology, and Medicine*, **5**, 106 (2009).
- [69] A. Nel, L. Mdler, D. Velegol, T. Xia, E. Hoek, P. Somasundaran, F. Klaessig, V. Castranova, and M. Thompson, *Nature Materials*, **8**, 543 (2009).
- [70] S. De Paoli Lacerda, J. Park, C. Meuse, D. Pristiniski, M. Becker, A. Karim, and J. Douglas, *ACS Nano*, **4**, 365 (2010).
- [71] G. Storm, S. Belliot, T. Daemen, and D. Lasic, *Advanced Drug Delivery Reviews*, **17**, 31 (1995).
- [72] D. Owens III and N. Peppas, *International Journal of Pharmaceutics*, **307**, 93 (2006).
- [73] X. Huang, I. H. El-Sayed, W. Qian, and M. A. El-Sayed, *J. Am. Chem. Soc.*, **128**, 2115 (2006).
- [74] H. Liao and J. Hafner, *Chem. Mater.*, **17**, 4636 (2005).

- [75] C. Loo, A. Lowery, N. Halas, J. West, and R. Drezek, *Nano Letters*, **5**, 709 (2005).
- [76] G. Hermanson, in *Bioconjugate techniques* (Academic Press Inc., New York, 1996) pp. 593–605.
- [77] D. A. Handley, in *Colloidal Gold: Principles, Methods, and Applications*, edited by M. A. Hayat (Academic Press Inc., New York, 1989) pp. 13–32.
- [78] M. Eghtedari, A. V. Liopo, J. A. Copland, , A. A. Oraevsky, and M. Motamedi, *Nano Lett.*, **9**, 287 (2009).
- [79] S.-S. Chang, C.-W. Shih, C.-D. Chen, W.-C. Lai, and C. Wang, *Langmuir*, **15**, 701 (1999).
- [80] S. Link, C. Burda, M. Mohamed, B. Nikoobakht, and M. El-Sayed, *Journal of Physical Chemistry A*, **103**, 1165 (1999).
- [81] C. Didychuk, P. Ephrat, A. Chamson-Reig, S. Jacques, and J. Carson, *Nanotechnology*, **20** (2009).
- [82] L. Chen, C. Wei, J. Souris, S. Cheng, C. Chen, C. Yang, P. Li, and L. Lo, *Journal of Biomedical optics*, **15**, 016010 (2010).
- [83] Y.-S. Chen, W. Frey, S. Kim, K. Homan, P. Kruizinga, K. Sokolov, and S. Emelianov, *Optics Express*, **18**, 8867 (2010).
- [84] I. Gorelikov and N. Matsuura, *Nano Letters*, **8**, 369 (2008).